Studies of surface diffusion and growth on Cu(111) by means of thermal energy atom scattering

2002 J. Phys.: Condens. Matter 14 6155

(http://iopscience.iop.org/0953-8984/14/24/314)

INSTITUTE OF PHYSICS PUBLISHING JOURNAL OF PHYSICS: CONDENSED MATTER

J. Phys.: Condens. Matter **14** (2002) 6155–6172 PII: S0953-8984(02)36115-0

Studies of surface diffusion and growth on Cu(111) by means of thermal energy atom scattering

J J de Miguel[1,3], **J Camarero**[2] **and R Miranda**[1]

[1] Departamento de Física de la Materia Condensada and Instituto de Ciencia de Materiales 'Nicolás Cabrera', Universidad Autónoma de Madrid, Cantoblanco, 28049-Madrid, Spain
[2] Laboratoire Louis Néel, CNRS, BP 166, 38042 Grenoble Cedex, France

E-mail: juanjose.demiguel@uam.es

Received 22 April 2002
Published 31 May 2002
Online at stacks.iop.org/JPhysCM/14/6155

Abstract

Some of the special characteristics of thermal energy atom scattering make it a uniquely adapted technique for investigations on diffusion and growth. In this work we review some recent results obtained during homoepitaxial and heteroepitaxial growth, both on bare substrates and assisted by a surfactant layer. We describe the fundamentals of the technique and the method of analysis, putting special emphasis on the information that can be obtained about important physical parameters such as Ehrlich–Schwoebel barriers, surface and edge diffusion, step bunching, and interdiffusion at heteroepitaxial interfaces. We also show examples of how diffusion and growth can be tailored by different means, such as using surfactants.

1. Introduction

Research on epitaxial growth and related issues has been boosted in recent years, with renewed interest driven by the prospects of technological applications. The quest for new materials with artificial, nanometre-sized structures and custom-designed properties relies heavily on our ability to identify the atomic-scale processes that ultimately control these samples' morphology. Epitaxial growth is carried out in conditions of very high supersaturation [1], and the artificial, low-dimensional systems prepared are metastable. In such out-of-equilibrium conditions kinetic parameters play a crucial role; in particular, the mobility of the deposited adatoms is directly responsible for many structural features. For instance, the preparation of crystalline superlattices demands a strict control of interfacial roughness, layer thicknesses, and interface structure [2]. More recently, the focus has shifted towards self-organized systems [3–5], for which a detailed knowledge of strain relaxation and segregation kinetics is a must.

[3] Author to whom any correspondence should be addressed.

In all cases, surface diffusion is at the heart of all relevant phenomena. Among the different experimental techniques employed in studies of diffusion and growth, thermal energy atom scattering (TEAS) has proven to be one of the most powerful for obtaining valuable quantitative information on growth kinetics and energetics [6, 7]. In this paper we discuss our method for analysis and interpretation of the data and present several examples illustrating the technique's capabilities.

2. Experimental system

The substrate used in all the experiments reported in this paper was a Cu(111) single crystal. It has a miscut angle of $\sim 1^\circ$ and has been used in UHV for several years. It was routinely cleaned by cycles of Ar^+ bombardment (500 eV, 5 μA cm^{-2}) and annealing at 500 °C. The sample temperature was determined by a chromel–alumel thermocouple pressed against the crystal edge.

Cu and Pb were evaporated from water-cooled Knudsen cells. The crucible temperature was measured by a thermocouple attached to it; this reading was fed to a temperature controller which regulated the output of the power supply. For Co we used home-made electron bombardment evaporators, also equipped with water-cooled screens. The deposition rates have been calibrated from the layer-by-layer intensity oscillations observed in the experiments employing Pb as surfactant [8].

The He source, of the Campargue type, provides a beam of momentum $k_i = 11$ Å^{-1} ($\lambda = 0.57$ Å), highly monochromatic ($\Delta k_i/k_i = 0.01$), with 1.0 mm diameter at the surface. It is modulated by a piezo-driven chopper vibrating at $\sim$240 Hz, and detected by a quadrupole mass analyser equipped with a channeltron multiplier whose analogue output is processed by a lock-in amplifier. The detector can be moved inside the vacuum chamber to change the incidence angle and select the desired interference conditions. As instrumental response function we use the experimental profile of the primary He beam, depicted in figure 1. It has Gaussian shape, with an FWHM of 0.65°. The system's base pressure is in the 10^{-10} Torr range, and it is further furnished with LEED and AES facilities.

3. Methodology

3.1. Basic concepts

Probably the most interesting feature of He-atom scattering for its application to studies of surface diffusion and growth is its high sensitivity to surface defects. This is a direct consequence of several facts, among which one should emphasize the nil penetration depth of the impinging He atoms into the substrate and their large cross section for scattering from defects. These properties are in turn mainly due to the low (thermal) energy of the incident beam, which typically ranges between 20 and 100 meV, and to the large extent of the overlap between the wavefunction of the incoming He atoms and the surface electronic density. The basic details of the atom–surface interaction have been worked out in a number of studies [9–11]. For our purpose it suffices to mention a few facts. First, the small atomic mass of He favours elastic dispersion. Also, the scattering process takes place at a distance of 3–4 Å from the cores of the surface atoms [12–14], which explains the nearly total absence of multiple-scattering events and thus enables us to analyse the data using kinematic diffraction theory. Finally, this technique is totally non-destructive, due to the low kinetic energy and lack of chemical reactivity of the probe atoms. It can therefore be safely used *in situ*, for studies of the evolution of surface morphology in real time during deposition [15, 16].

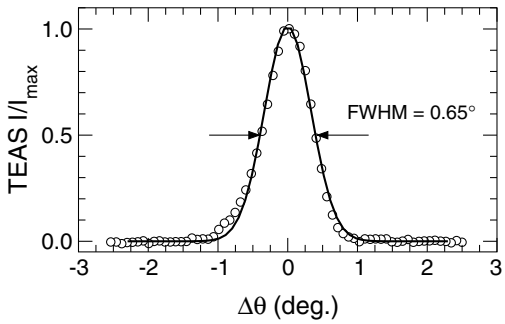

Figure 1. The angular profile of the primary He beam. The solid curve is a Gaussian fit to the data (○).

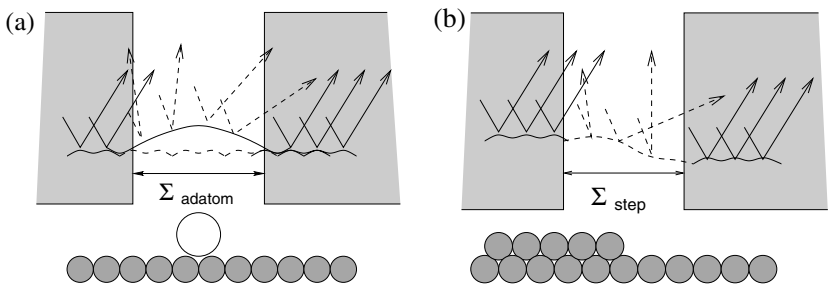

Figure 2. Schematic representations of the cross section for diffuse scattering Σ of (a) an adatom adsorbed on a surface and (b) an atomic step. Only He atoms scattered off the shaded areas reach the detector and contribute to the specular intensity measured in a typical TEAS experiment.

The experiments that will be described in the following have all been conducted by monitoring the changes in the intensity of the specular beam. This peak contains all the relevant information about the height distribution on the surface, and is by far the most intense one: for compact faces of transition metals, and due to the delocalization of the conduction electrons, the surface electronic density is quite spread out and shows a very small corrugation. In these cases, the intensity of higher-order diffracted peaks is at most 10^{-4} times that of the (00) peak [17].

The principle underlying the measurements relies on the concept of the cross section for diffuse scattering from surface defects, as illustrated schematically in figure 2. Both point objects such as adatoms or vacancies (panel (a)) and extended ones such as steps (panel (b)) cause distortions in the periodicity of the surface that cause He atoms scattered within these regions to be directed outside the specular direction, adding to the diffuse background intensity. The cross section Σ is defined as the total distorted area surrounding the object in the first case. For steps, in contrast, Σ represents the width affected by the perturbation, per unit step length. Hence, any losses in the sample reflectivity with respect to the clean surface can be translated into the corresponding increases of the defect concentration, provided that the values of the cross sections are known. Σ is typically one order of magnitude larger than the geometrical size of the dispersing object: for instance, it amounts to 123 Å^2 for a single CO molecule adsorbed on Pt(111) [18] or 12 Å for monatomic steps on Cu(100) [19, 20]. The large magnitude of these cross sections explains the high sensitivity of TEAS.

It is important to note that the effect of diffuse scattering from defects can be observed independently of the scattering conditions, either in-phase or out-of-phase. In the latter case, TEAS experiments in principle sense the balance of areas exposed at different heights within the extents of the diffractometer's transfer width ω. This magnitude can be found using the following expression [11, 21]:

$$\omega = \frac{\lambda}{(\Delta\theta)\theta_i \cos\theta_i} \tag{1}$$

where λ is the He beam's wavelength, θ_i is the incidence angle, and $\Delta\theta$ represents the diffractometer's angular dispersion, which can be determined by measuring a profile of the incident beam such as the one displayed in figure 1. In our experiments, θ_i is typically between 70° and 80°, giving us transfer widths of the order of 150 Å. The average size of atomic terraces in well-prepared, non-vicinal single-crystal surfaces is usually larger than ω. For this reason, the initial surface prior to starting growth reflects a non-zero intensity. We shall come back to this issue later on, when discussing step bunching and debunching in section 4. On the other hand, the nucleation and lateral growth of two-dimensional islands of smaller size favours the cancellation of the amplitudes scattered from different atomic levels and causes a reduction in the diffracted intensity.

3.2. Observation of different growth modes

The type of growth can be identified by observing the behaviour of the specular intensity as deposition proceeds. Restricting ourselves to layer-by-layer or Frank–van der Merwe growth [22], and depending on the adatoms diffusivity, several modes can be defined. The prototypical cases are schematically depicted in figure 3, together with the expected evolution of the diffracted intensity. In the first case shown (figure 3(a)), both interlayer and intralayer diffusion are reduced; a large number of small islands are formed with a high border-to-area ratio. Also, many atomic levels rapidly become populated because atoms that landed on previously formed islands can hardly cross descending edges. The step density thus steadily increases, resulting in a continuous reduction of the diffracted intensity, as indicated in the figure. When diffusion across steps is easy, each atomic level tends to fill up before the next one starts to grow. Surface roughness then varies periodically, reaching a maximum for layer half-filling and a minimum at the completion of each level. This behaviour gives rise to the well-known periodic oscillations of the specularly reflected intensity [23, 24], as illustrated in figure 3(b). When the in-plane mean free path of the deposited adatoms is long enough, they can reach the natural steps of the substrate and stick to them before nucleating islands on the terraces. The film then grows by continuous advancement of those steps and the balance of areas on each atomic level remains unaltered, so for most techniques the intensity diffracted under destructive interference conditions will be practically constant. TEAS, however, thanks to the large cross sections for diffuse scattering from steps, can easily detect the increasing roughness in the edges as they advance across the surface. This phenomenon manifests itself in a relatively slow decrease of scattered intensity (see figure 3(c)), and takes place when adatom diffusion along the steps is limited, as will be demonstrated in section 5. Only with unlimited diffusion parallel to the edges can the latter's initial smooth morphology be maintained indefinitely during growth, giving as a result a truly constant TEAS intensity, as depicted in figure 3(d).

3.3. Kinetic growth model

For a detailed, quantitative analysis of the experiments we have developed a procedure that takes full advantage of the kinematic nature of the He–surface scattering process. We start

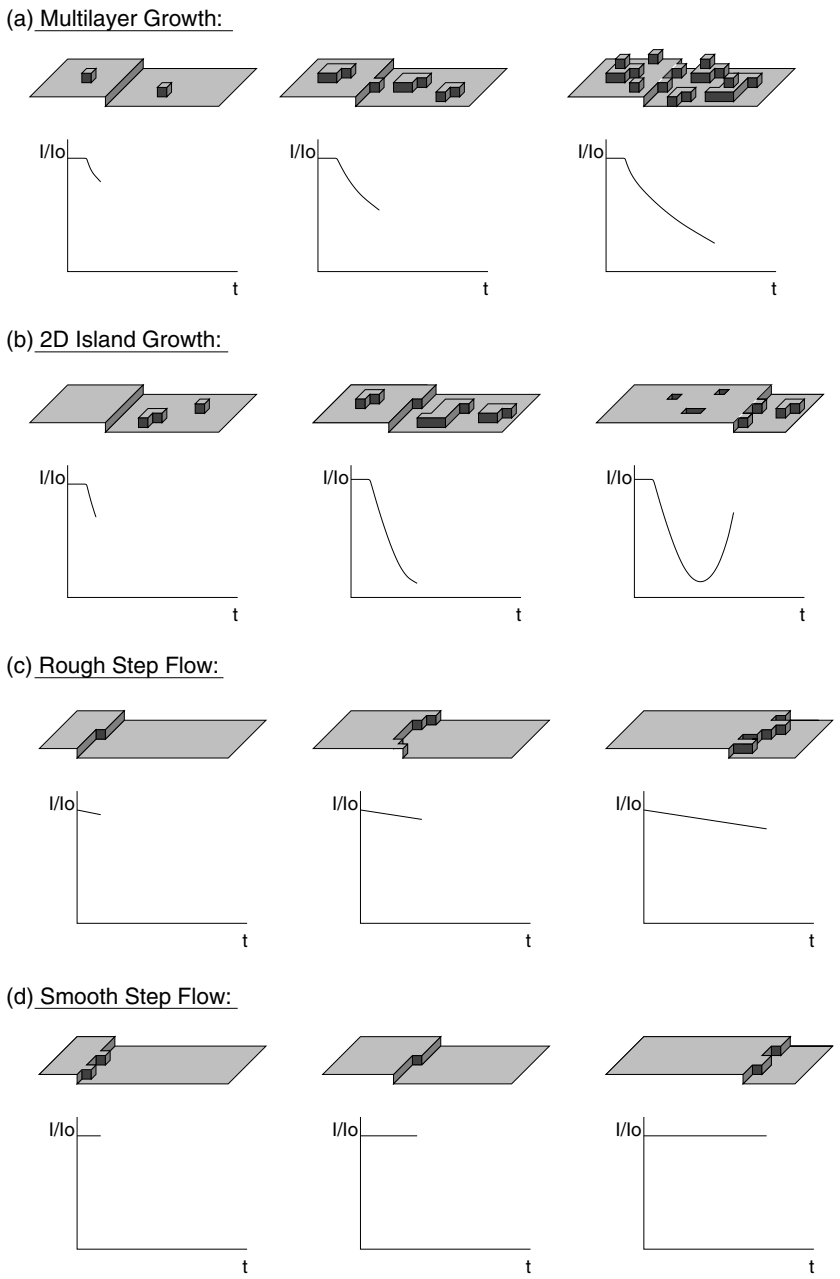

Figure 3. Schematic representations of the different growth modes as observed with He-atom scattering.

by constructing an appropriate kinetic growth model based on the one proposed by Cohen *et al* [25]. A set of differential rate equations describe the variations in the occupation of each atomic level; a few adjustable parameters are introduced to capture the essential features of the problem. In their simplest form, for a homoepitaxial system, the equations take the following form:

$$\begin{aligned}
&\Theta_0 = 1.0 \\
&\frac{\mathrm{d}\Theta_1}{\mathrm{d}t} = R(\Theta_0 - \Theta_1)(1 - W_{\mathrm{DZ}}) \\
&\frac{\mathrm{d}\Theta_i}{\mathrm{d}t} = R[(\Theta_{i-1} - \Theta_i) + \alpha_i(\Theta_i - \Theta_{i+1}) - \alpha_{i-1}(\Theta_{i-1} - \Theta_i)] \qquad (i \geqslant 2).
\end{aligned} \tag{2}$$

The terms in the right-hand side of the last equation correspond to the different processes that cause changes in the layer occupations: the first one accounts for direct deposition onto the uncovered area of each level, and the last two describe the fluxes of atoms arriving from a higher level and falling towards a lower one, respectively. The coefficients α_i control the probability of interlayer diffusion, and are defined as follows:

$$\alpha_i = A\frac{d_i(\Theta_i)}{d_i(\Theta_i) + d_{i+1}(\Theta_{i+1})} \tag{3}$$

where

$$d_i(\Theta_i) = [\Theta_i(1 - \Theta_i)]^{1/2}. \tag{4}$$

In the last equation, $d_i(\Theta_i)$ is defined so as to take a symmetric shape about layer half-filling; it thus keeps track of the varying average distance between steps at different stages during deposition. The eventual existence of Ehrlich–Schwoebel (ES) barriers [26,27] hindering step crossings is described by means of a single parameter A.

Our model incorporates another important feature, namely the existence of steps on the clean surface due to the—unavoidable—sample miscut. During growth, a fraction of the deposited material will land close enough to the ascending steps to be able to reach them and stick there, instead of nucleating islands on the terraces. This results in the appearance of the so-called 'capture' or 'denuded zones', stripes deprived of islands near each step, as illustrated in figure 4. Obviously, the width of these zones, which we denote by W_{DZ}, is directly related to basic growth parameters such as the adatom diffusivity or the critical nucleus size [28]. This effect is responsible for the experimentally observed transition from a growth mode based on the nucleation of two-dimensional (2D) islands to step flow, with increasing atom mobility; in our model, it is included in a very simple way: in (2) we modify the equation for θ_1 by introducing the factor $(1 - W_{\mathrm{DZ}})$ in the right-hand term. Thus, the kinetic growth model is applied only to the fraction of the surface that is not covered by the denuded zones; in these areas, in contrast, the surface morphology does not change and therefore we assume that the reflectivity for the He beam remains unchanged. The rate equations for the second and further layers need not be modified, since they already refer to the value of Θ_1. The transition to step flow with its characteristic increase of the average diffracted intensity emerges then trivially from this model as W_{DZ} approaches unity.

3.4. Data fitting method

Our procedure to analyse growth data obtained by means of TEAS is graphically described in figure 5. We start by choosing some values for the free parameters (A, W_{DZ}) and solving the system of rate equations (2)–(4). As output we obtain the continuous evolution of the atomic level occupations during deposition; a characteristic example is depicted in figure 5(a). With this information to hand, it is straightforward to calculate the diffracted intensity in the kinematic approximation, simply adding with the appropriate phases the amplitudes scattered by the uncovered fraction of each level and taking the square of the sum:

$$\frac{I}{I_0} = \left[\sum_{j=0}^{\infty}(\Theta_j - \Theta_{j+1})\exp(\mathrm{i}k_\perp z_j)\right]^2. \tag{5}$$

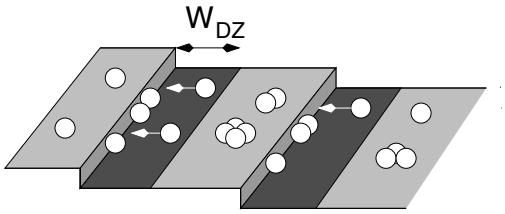

Figure 4. A schematic representation of the denuded zones near the surface steps, where island nucleation is suppressed.

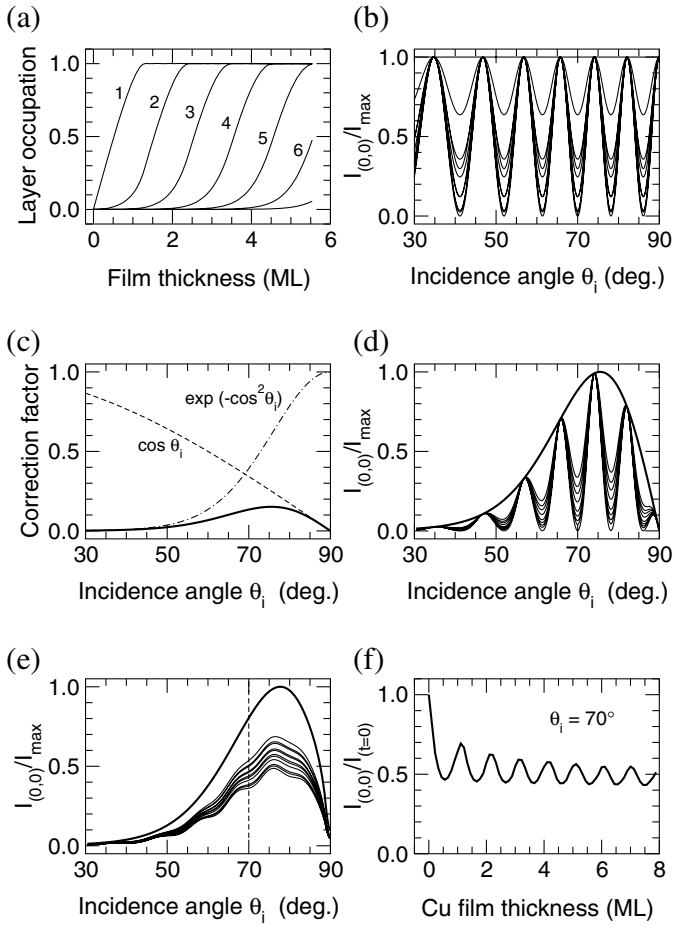

Figure 5. Stages in the procedure used to analyse TEAS growth data: (a) solution of the rate equations (2) and obtaining of layer occupations as a function of deposited thickness; (b) calculation of theoretical θ–2θ scans for the whole range of thicknesses; (c) angle dependence of the intensity corrections for thermal damping (Debye–Waller factor, — · —), grazing incidence (- - - -), and combination of the two (——); (d) θ–2θ scans corrected by those factors and (e) after convolution with the instrumental response function (see figure 1); (f) construction of the theoretical uptake curve by taking the values of the θ–2θ curves at the appropriate incidence angle. This simulated curve is compared with the experimental data and the procedure is repeated with modified parameters until a satisfactory agreement is reached.

This calculation can be done for a range of incidence angles and for a series of different film thicknesses; in this way we obtain a set of ideal θ–2θ scans such as those presented in figure 5(b). In order to compare these results with the experimental data, several instrumental corrections must be introduced. In particular, there exist two factors that depend on the incidence angle and are not accounted for by the instrument response function. Inelastic scattering due to thermal vibrations causes a damping of the diffracted intensity that is more important for normal incidence; its effect can be described in a first-order approximation by multiplying the intensity by the well-known Debye–Waller factor, $f_{\mathrm{DW}} = \exp[-(\Delta k_{\perp})^2 \langle u_z^2 \rangle]$ [29]. Following the convention for TEAS, we measure the incidence angle with respect to the surface normal; therefore, $f_{\mathrm{DW}} \sim \exp(-\cos^2 \theta_{\mathrm{i}})$. Also, at very grazing incidence the cross section presented by the canted sample is proportional to $\cos\theta_{\mathrm{i}}$, and it eventually becomes smaller than the finite width of the incident He beam. A fraction of the latter then does not hit the surface, and the specular signal is consequently reduced. The shapes of these two factors are shown in figure 5(c); the combination of the two of them produces the envelope curve depicted as a solid line. After applying this correction to the θ–2θ scans calculated above, we obtain sets of curves like the one plotted in figure 5(d). In the next step we have to incorporate other instrumental limitations: energy (momentum) spread and angular width of the incident beam, finite detector aperture, etc. We include these effects by convolving the θ–2θ scans with the experimental profile of the incident beam (see figure 1), which contributes to mixing different interference conditions in the measurements and partially washing out the features in the θ–2θ curves. These are shown in figure 5(e). Finally, the calculated uptake curve—figure 5(f)—can be constructed by taking the values of all those scans for a particular incidence angle, as a function of film thickness. This theoretical curve is compared with the experimental data, and the whole procedure is repeated varying the parameters in the growth model until a satisfactory agreement is reached.

In the following sections we shall present several examples demonstrating the capabilities of our method of analysis and the usefulness of TEAS for characterizing different interesting examples of surface morphology and epitaxial growth.

4. Kinetic step bunching and debunching

The early atomistic growth theories, and most notably the BCF model [30], did not consider the possibility of asymmetric rates of atomic incorporation into the surface steps. After the first experimental observation of such an effect [26] it soon became clear that it could have a profound influence on surface morphology [27]. This phenomenon is usually described in a simplified way in terms of the so-called ES barrier: the effective additional energy required by an adatom to cross a descending step. The origin of this barrier is the reduced coordination that the diffusing adatom feels during its transit across the edge. Figure 6 presents an example corresponding to the [100] step of a Cu(111) surface. The energy curve has been calculated by means of static relaxation [31] (a type of molecular dynamics simulation with frozen time), using embedded atom (EAM) interatomic potentials [32]. A Cu adatom was placed at different fixed positions on the surface and the minimum-energy configuration was found by relaxing the rest of the atoms in the simulated sample. It is clear from the figure that the energetic cost of crossing this step is much larger than the activation energy for diffusion on the terraces. In reality, the situation is more complex: atoms usually cross the steps by an exchange mechanism, pushing forward an edge atom and taking its position [33]. This process involves a concerted motion of at least two atoms. Also, instead of a barrier localized at the edge, FIM experiments have shown that the perturbations in the energy barriers for diffusion extend several unit cells from the step [34]. In any case, it now seems that these barriers are quite common, and their

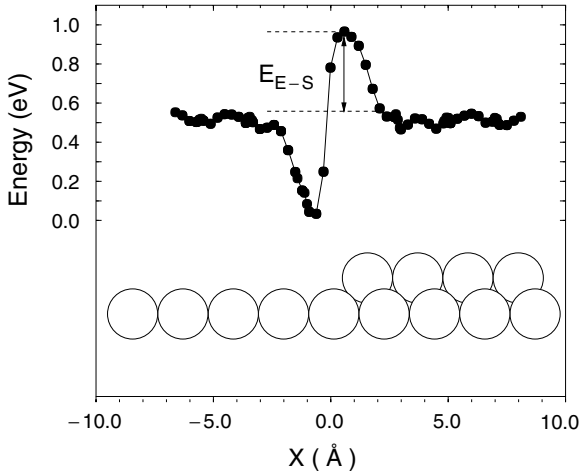

Figure 6. An example of an ES barrier: the graph shows the potential energy felt by a Cu adatom diffusing by hopping above the Cu(111) surface and across a [100]-type monatomic step. The ES barrier is the excess energy needed by the adatom to cross the edge. The curve has been calculated by static relaxation using EAM interatomic potentials [31].

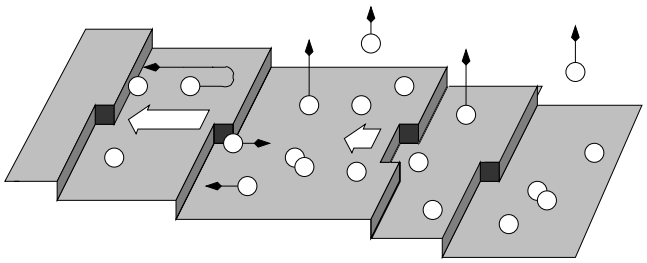

Figure 7. A schematic representation of sublimation from a vicinal surface and the different velocities of step recession that cause step bunching when interlayer diffusion is suppressed.

effect is specially noticeable on compact crystal faces, where the activation energy for surface diffusion is low [8].

The existence of ES barriers hindering interlayer diffusion can have a substantial influence on surface morphology, even before starting growth. The usual procedure used to prepare clean, well-ordered surfaces under ultrahigh vacuum (UHV) consists of applying cycles of Ar^+ sputtering and high-temperature annealing. During the latter, significant sublimation from the surface can take place. The atomistic processes involved are depicted schematically in figure 7. Single atoms detach from kink sites along the surface steps. If step crossings are forbidden, these atoms are confined to the lower terrace adjacent to their step of origin. An equilibrium density of monomers is reached when the rate of adatom impingement onto the step equals that of detachment. At this stage, the velocity of the receding steps is controlled by the rate of sublimation of adatoms into the vacuum. Starting with an ideal surface with terraces of equal size, all steps are expected to move backwards with the same velocity. However, random fluctuations create differences in terrace size that become rapidly amplified. As indicated in figure 7, larger terraces can accept more adatoms and therefore their ascending steps recede faster. In this process, wide terraces grow wider at the expense of narrow ones. Finally, faster steps catch up with the slower ones, forming groups or bunches.

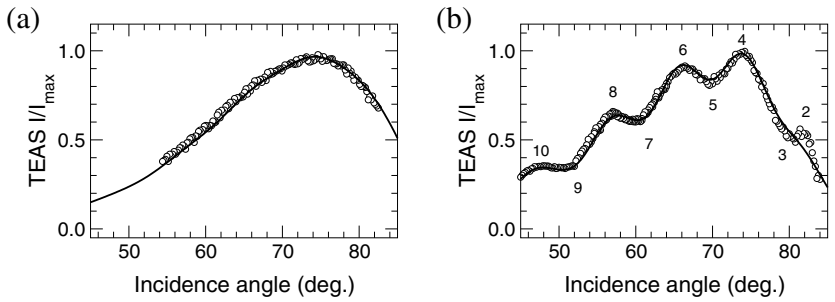

Figure 8. (a) A TEAS θ–2θ scan obtained on a clean Cu(111) surface (1° miscut) with step bunches. The solid curve is a kinematic fit to the data (○), assuming an average terrace size of 1500 Å, which implies ∼12 steps per bunch. (b) A θ–2θ scan on the same surface after deposition of 5 ML of Cu in the step-flow regime. The fit (——) has now been obtained for a terrace width of 120 Å, similar to the nominal value. The interference maxima and minima visible in this case have been labelled according to their order n.

The appearance of step bunches can easily be detected using TEAS. Since the average sample orientation cannot change, the morphology of the bunched surface consists of very large terraces separated by groups of very narrow ones. These latter barely contribute to the diffracted intensity, because a great part of them is covered by the cross section for diffuse scattering from the steps forming the bunch. Therefore, the flat areas in the sample become much larger than their nominal value, according to the sample miscut. In particular, they can be several times larger than the instrument's transfer width ω. In that case, the measurements are insensitive to the interference conditions. This is demonstrated by the data presented as open circles in figure 8(a). This θ–2θ scan measured on a Cu(111) surface with step bunches shows no features associated with the interference between adjacent terraces. The solid curve is a fit to the data using the method outlined in the previous section, assuming that the width of the flat regions between the steps is 1500 Å. This value corresponds to ∼12 steps per bunch.

The step bunching process is purely kinetic, and therefore it can be reversed. It suffices to invert the sign of the chemical potential and the step velocity, i.e., to deposit material onto the surface instead of sublimating it. Deposition under conditions of high atomic mobility results in step-flow growth. With jumps to lower terraces forbidden by the high ES barriers, all atoms landing on a given terrace have to stick to its ascending step. Obviously, the narrow terraces forming the bunches receive very few adatoms, and their steps move forward slowly. In contrast, the large number of adatoms arriving at the wide terraces left between the bunches have to adhere to the first step in the upper group. This step advances rapidly and leaves the bunch. With this displacement, the lower terrace shrinks and the upper one expands; this causes a reduction in the supply of adatoms to the first step, whose velocity decreases gradually. At the same time, the second step in the bunch starts to receive more atoms and breaks away from it. The whole process is portrayed in figure 9: these snapshots show the evolution of a one-dimensional train of steps, initially bunched, as deposition proceeds. The step positions (or layer occupations) have been obtained by integration of the rate equations (2)–(4) assuming random deposition and diffusion unlimited within the terraces but zero across steps.

It is interesting to note from figure 9 that, in order to eliminate the bunches and recover a distribution of nearly equidistant steps, it is necessary to deposit as many monolayers (MLs) as roughly half the number of steps in each bunch. Our measurements on Cu(111) also confirm this assertion. The θ–2θ scan presented in figure 8(b) was measured on the same surface as described above, but after having grown 5 ML of Cu in step-flow mode. Now the maxima

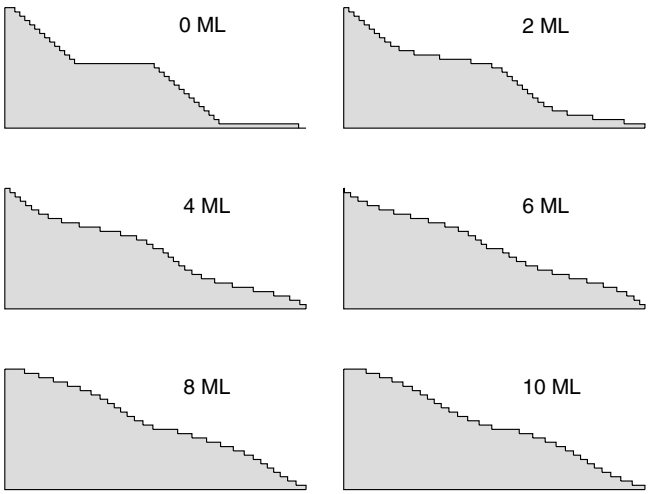

Figure 9. Kinetic step debunching. The equilibrium terrace width is recovered after growing in step-flow mode a thickness roughly similar to half the bunch size. The evolution of level occupations has been obtained by solving the system of rate equations described in the text.

and minima due to interference between adjacent terraces can be clearly seen; they have been labelled according to their Bragg order. Their angular positions correspond to an interlayer spacing $h_{\mathrm{Cu}(111)} = 2.08 \pm 0.02$ Å, in agreement with bulk values [7]. The fit to the data (solid curve) indicates that the average terrace width in this case is 120 Å, in excellent agreement with the nominal value corresponding to the sample's vicinality.

5. Step roughening and edge diffusion

It is commonly assumed that, when their mobility is high enough, adatoms deposited on a surface will be able to reach the existing steps due to the sample's miscut and stick to them, finding the appropriate minimum-energy positions such that the edges maintain a smooth shape as they advance across the surface in what is called the step-flow growth mode. Nevertheless, this is not always the case. The diffusing adatoms adsorb at random positions along the edges, and for these latter to remain straight it is necessary that those atoms can move parallel to the step line seeking sites with higher coordination. If the activation energy for edge diffusion is higher than that for in-plane motion (as happens usually for fcc (111) faces [31,35]) then there will be no island nucleation at the terraces, but the advancing steps will progressively roughen as deposition proceeds. This is the so-called 'Bales–Zangwill' effect [36], and constitutes a particular case of diffusion-limited aggregation in one dimension.

The step roughness caused by this limited step diffusivity is amplified if there exist high ES barriers hindering interlayer diffusion. The process can be described as follows: starting with a smooth propagating step, statistical fluctuations cause the appearance of protrusions along the edge line. If the flux of adatoms coming to join the step from the upper terrace is negligible, then all the material arriving at the step must come from the lower one. The protrusions have a larger probability of trapping incoming adatoms than the cavities between them: then they grow longer, forming dendrites. A characteristic surface morphology during rough step-flow growth is shown in figure 10: this is the result of a simple kinetic Monte Carlo (MC) simulation assuming zero interlayer diffusion and limited mobility along the steps.

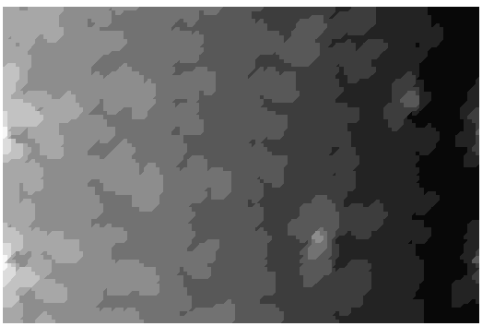

Figure 10. A snapshot of a kinetic MC simulation demonstrating the appearance of dendritic edge shapes during step-flow growth with no step crossings and limited diffusion along the steps.

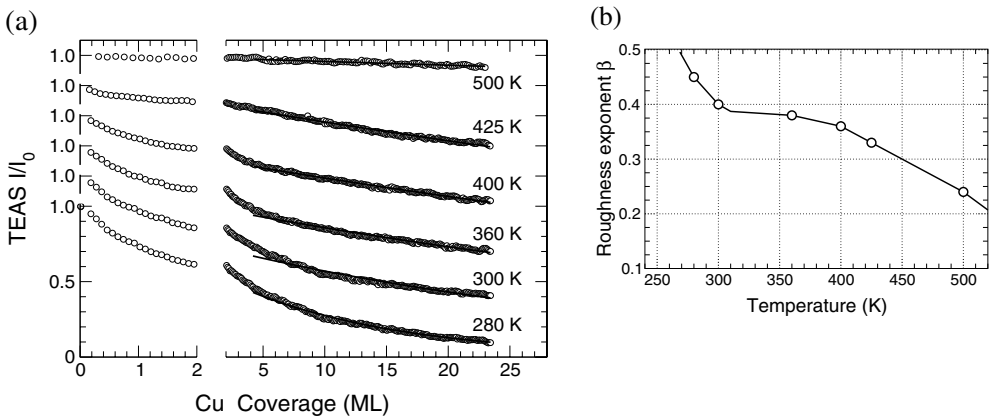

Figure 11. (a) TEAS uptake curves showing the variation of the specular intensity during Cu deposition on a Cu(111) surface with step bunches. After an initial transient during step debunching, the data (○) can be fitted with power laws of the type $W = t^{\beta}$ (——) as predicted by kinetic roughening theories. (b) The temperature dependence of the roughness exponent β mirrors the changes in atomic diffusion along the steps (see the text).

Cu(111) fulfils all requirements for displaying rough step flow: diffusion along the steps is slower than on the terraces [31, 35] and interlayer diffusion is practically negligible, as will be shown in more detail in section 6. Typical TEAS experiments of homoepitaxial growth on a Cu(111) surface containing step bunches are presented in figure 11. The measurements show the evolution of the specular intensity, diffracted at the out-of-phase condition, during deposition at different substrate temperatures. The data in figure 11 (open circles) are presented separated into two regions: the early stages of growth (Θ_{Cu} below 2 ML) are dominated by the nucleation of islands on the larger terraces, while at the same time the step bunches are dissolving. In this range of thicknesses the data can be analysed with the aid of our growth model described in section 3; some representative examples will be presented below. For film thicknesses above 5 ML, the step bunches have disappeared and the whole surface is growing in rough step-flow mode. The steady decrease of the TEAS intensity indicates that additional defects are being accumulated at the surface.

Kinetic roughening theories predict a power-law increase of the roughness with deposition time: $W = t^{\beta}$ [37, 38], where β is the so-called *'roughness exponent'*, whose value depends on

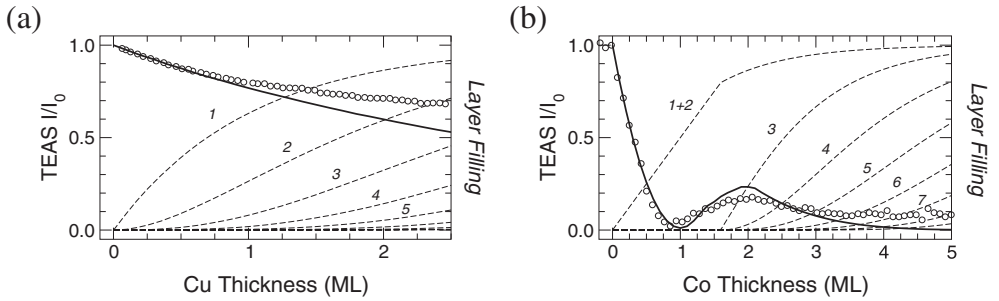

Figure 12. TEAS characterization of the growth of (a) Cu, and (b) Co on Cu(111) at room temperature. The data (○) have been fitted using the procedure described in the text. Also shown in the figure are the fit (——) and the gradual filling of atomic layers (- - - -), as obtained from it. For Co, the first and second atomic layers grow simultaneously, forming a mixed Co–Cu bilayer.

the details of the diffusion processes involved. The decrease in the TEAS intensity can easily be correlated with the total length of steps on the surface [6]. Using this, we have been able to fit the high-coverage region of our data with power-law expressions (see the solid curves in figure 11(a)). Different exponents β were obtained, depending on the sample temperature; they are depicted in figure 11(b). The physical meaning of these values is discussed in full detail elsewhere [7, 37]; here we shall give only a brief account of it. At low temperature, diffusion parallel to the steps is practically inhibited, and β tends to $1/2$. At the opposite limit, $\beta = 0$ indicates unlimited edge diffusion and perfectly smooth steps. $\beta = 1/4$ is expected when atoms moving along the steps are able to cross kinks. Between 300 and 400 K, we find a plateau with $\beta = 3/8$, which corresponds to atoms diffusing along straight segments of steps but not being able to turn corners [39]. Therefore, the evolution of the values of β as a function of T provides information on the atomic-scale mechanisms of diffusion.

6. Surface diffusion, growth, and interface formation

In an atomistic description of growth the key processes are diffusion in all its flavours (interlayer and intralayer, parallel to the steps, etc) and nucleation. Besides, practical applications rely on the use of heteroepitaxial systems, for which an accurate control of the quality of interfaces is crucial. The power of TEAS in studying such problems lies in the wealth of information that can be obtained from a single measurement and a relatively simple analysis of the data.

Two representative examples of epitaxial growth are displayed in figure 12. The open circles in these graphs show a TEAS measurement of the specular intensity during deposition of (a) Cu and (b) Co on Cu(111). The substrate temperature was 300 K in both cases, and the deposition rates 1.5 ML min^{-1} for Cu and 1.2 for Co. The dashed curves describe the evolution of individual layer occupations that produces the fits to the data represented as solid curves. They have been obtained using the kinetic growth model given by equations (2)–(4), and the fitting procedure described in section 3 and in figure 5. Despite the quite different shapes of the two uptake curves, the actual morphologies of these films are quite similar. In both cases, the fits were obtained setting $A = 0$ in the rate equations, implying that the ES barriers are high and interlayer diffusion is non-existent. With random deposition, each layer receives a number of adatoms proportional to the uncovered area of the level immediately below, and the filling of atomic levels follows Poisson statistics [40]. These films are expected to grow forming pyramids. However, this only applies to the fraction of deposited material that grows

by nucleation of islands. The high reflectivity of the sample during Cu deposition is explained by the large size of the denuded zones: $W_{DZ} = 0.86$, which means that the mean free path of Cu adatoms is large and most of the deposited material grows in the step-flow mode. In fact, the step debunching process described in section 8 is the reason for the deviation of the fit from the experimental data above 1 ML thickness. A detailed analysis of the temperature dependence of W_{DZ} in the low-coverage limit yields an activation energy $E_{DZ} = 11 \pm 6$ meV [7]. This energy can be directly related to the activation energy for surface diffusion [41–43] through nucleation theory [1, 28, 44]; a detailed discussion can be found elsewhere [7].

During Co deposition, in contrast, the width of the denuded zones is negligible. This is not an indication of slow in-plane diffusion, but is rather related to the existence of alloying at the Co–Cu interface. The atomistic mechanisms of intermixing have been revealed by computer simulations [45]. Co atoms diffuse by hopping with great mobility on the Cu(111) face and mix preferentially at descending steps. The first alloyed Co atoms act as preferential nucleation sites for others arriving later; as a result, all atomic steps in the surface are decorated in the very early stages of deposition with clusters made up of a mixture of Co and Cu [46, 47]. The size of these clusters does not increase indefinitely: it seems to saturate at some point, indicating that the decorated steps are passivated against further incorporation of arriving Co adatoms. Consistently with our TEAS measurements, no denuded zones have been observed in STM experiments on the same system [46, 48].

Interdiffusion is also responsible for the other major difference between these two systems: while Cu grows on Cu(111) at all stages in single atomic layers, the islands formed at the Co–Cu interface have double atomic height, and contain a mixture of deposited Co and Cu etched from the surface. The existence of bilayer islands is easily detected by TEAS: the layer filling curves in figure 12(b) clearly show that the first two atomic layers populate simultaneously. The presence of Cu mixed with Co inside the islands cannot be derived from the He scattering measurements, but it has been confirmed by STM observations with CO titration [46] and ion scattering experiments [49]. The etching of surface atoms and the formation of the bilayer islands takes place as single-layer aggregates of pure Co become unstable and break up [45], apparently trying to relieve their misfit strain [50]. Once that the Cu substrate is completely covered, the growth of Co onto itself continues in a manner analogous to that of Cu on Cu.

7. Influence of surfactants on atomic diffusion

The absence of interlayer diffusion in the systems studied in the previous section produces very rough films, totally unsuited for practical applications. The electronic and magnetic properties of nanostructured materials are extremely sensitive to structural defects [51] and roughness [52]. It is therefore necessary to develop growth methods capable of overcoming these difficulties to produce layers of good structural quality. Many different approaches have been tried. For instance, irradiation with low-energy ions during deposition promotes layer-by-layer growth by breaking up small nuclei formed on the upper atomic levels [53]. Low-temperature deposition followed by gentle annealing seems to be effective at preventing interface alloying [54]. This method also enhances interlayer diffusion to some extent; the reduced in-plane mobility of the adatoms results in smaller islands with ragged edges, which are much easier to reach and cross for adatoms landing on top of them [55]. However, the short diffusive lengths involved impose severe limitations on the size and smoothness of the structures that can be prepared in this way.

In this section we attempt to give a brief overview of the effect of a surfactant on both homoepitaxial and heteroepitaxial growth, using for that purpose the same systems as were described above. A surfactant is an additive introduced in the growth process in order to

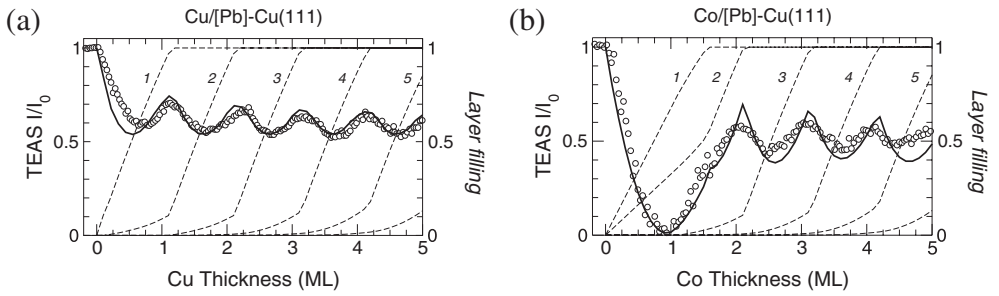

Figure 13. Growth of (a) Cu and (b) Co on Cu(111) at room temperature, assisted by one monolayer of Pb (○), and the fit to the data (——) using the procedure described in the text. In both cases, the surfactant induces layer-by-layer growth. The evolution of layer occupations is depicted with broken curves (– – –). In (b), the first intensity oscillation is missing due to the existence of some mixing at the Co–Cu interface, which results in the formation of islands with double atomic height. The amount of intermixing, however, is strongly reduced with respect to that for the layers grown without surfactant.

modify it in an appropriate way [56]. This method offers greater flexibility, because one can in principle try to act upon specific atomic processes without affecting others [45].

We have used Pb as the surfactant. When deposited on Cu(111) at 450 K, it forms a compact monolayer with a p(4 × 4) superstructure, with three Pb atoms per unit cell and a saturation coverage of 9/16 with respect to the substrate surface [57, 58]. A good surfactant must segregate efficiently to the surface of the growing layer, so as not to introduce any impurities in the film and also to maintain its activity indefinitely. This is the case with Pb: its surface free energy ($\gamma_{Pb} = 0.5$ J m^{-2} [59]) is much lower than those of either Co or Cu ($\gamma_{Cu} = 1.9$ J m^{-2}, $\gamma_{Co} = 2.7$ J m^{-2} [60]). When either of these two materials is deposited onto the Pb-covered substrate the surfactant layer tends to float to the surface, and the deposit gets buried below it. Molecular dynamics and MC simulations [61] have shown that this exchange process is very fast: the adatoms landing on the surfactant immediately sink through the nearest hollow site, without any lateral displacement. In-plane diffusion and nucleation of the growing material must take place below the surfactant layer, which completely alters the atomic processes involved and consequently the morphology and structure of the epitaxial film [62].

TEAS experiments enable us to characterize in full detail the surfactant effect. Figures 13(a) and (b) display uptake curves measured during Pb-assisted growth of Cu and Co, respectively. These data (depicted with open circles) must be compared with their counterparts in figure 12, for similar films grown without surfactant. The differences are striking. The oscillations in the specularly diffracted intensity demonstrate that the presence of the Pb layer induces layer-by-layer growth in two systems that otherwise grew in multilayer fashion. A quantitative analysis of the film structures can be obtained by fitting the experimental data with our method. With the appropriate growth parameters we obtain the fits shown as solid curves in both graphs. Remarkably, the fit to the intensity oscillations in both experiments required the same value of the parameter $A = 0.93$, very close to that for the unlimited interlayer diffusion that is characteristic for perfect layer-by-layer growth. This fact suggests that the probability of step crossing in these cases is entirely controlled by the presence of the surfactant layer, independently of the material being grown.

Our fit to the data in figure 13(a) also reveals a reduced width of the denuded zones, $W_{DZ} = 0.23$, as compared to that for the growth of Cu on clean Cu(111). This indicates that

in-plane mobility is considerably smaller in the presence of the surfactant, a finding that is consistent with former studies [8] showing that both Co and Cu atoms diffuse by the exchange mechanism [63, 64] on the Pb-covered surface instead of hopping as on clean Cu(111). In this way, the presence of the surfactant reduces intralayer mobility but favours interlayer diffusion, because the islands formed below the Pb layer are smaller. However, this surfactant-induced decrease in the in-plane diffusivity of the adatoms does not affect other kinetic processes such as edge diffusion: for instance, STM has proved that the islands formed below the Pb layer have compact and smooth borders [66].

In order to fit the data for heteroepitaxial growth (figure 13(b)) we had to modify our growth model of equations (2)–(4) to introduce two different denuded zone widths, instead of just one: $W_{\mathrm{DZ}}^{\mathrm{CoCu}}$ now applies only to the interface layer, where Co atoms diffuse and nucleate over the Cu substrate, while $W_{\mathrm{DZ}}^{\mathrm{CoCo}}$ is for the upper atomic layers, where Co is growing homoepitaxially onto itself. Still, it must be emphasized that the whole experimental curve is fitted using only three adjustable parameters. For the interface layer we obtain $W_{\mathrm{DZ}}^{\mathrm{CoCu}} = 0.05 \pm 0.05$, a value again close to zero, as for the growth of Co on Cu(111) without surfactant. The absence of the first intensity oscillation and the evolution of layer occupations (depicted as broken curves in figure 13) demonstrate that there are still a fraction of islands with double atomic height, although in much smaller proportion than in the former case, indicating that some amount of intermixing remains. The short diffusive length of the Co directly in contact with Cu could therefore be attributed to heterogeneous nucleation. In contrast, when Co diffuses over itself, one finds $W_{\mathrm{DZ}}^{\mathrm{CoCo}} = 0.15 \pm 0.10$. This value is comparable to, albeit smaller than, the one reported in the previous paragraph for Cu on Cu in the presence of Pb. This also hints that atomic diffusion in these cases is basically controlled by the surfactant layer. A systematic analysis of these issues will be presented in a forthcoming paper [65].

8. Summary

We have demonstrated the ample capabilities of TEAS for growth studies. This technique is especially well suited for real-time measurements during deposition, because of its high sensitivity to defects and its low energy, which precludes any damage to the surface of the growing film. Analysing the experimental data with an appropriate growth model and kinematic diffraction theory, a single uptake curve can offer a complete description of the evolution of the surface morphology as a function of film thickness. Several experimental results on the growth of Cu and Co on Cu(111), with and without surfactant assistance, have been presented as case study models to show the kind of information that can be obtained on different issues such as the existence of ES barriers against diffusion across atomic steps, kinetic step bunching and debunching, surface diffusion, interface formation, and the atomistic mechanisms of surfactant-induced layer-by-layer growth. The knowledge derived from these experiments is key for improving the quality and performance of novel, nanostructured materials.

Acknowledgment

This work has been supported by MCyT through Project Number BFM2001-0174.

References

[1] Venables J A, Spiller G D and Hanbücken M 1984 *Rep. Prog. Phys.* **47** 399

[2] See for instance:
Dhez P and Weisbuch C (ed) *Physics, Fabrication and Applications of Multilayered Structures (NATO ASI Series B, vol 182)* (New York: Plenum)

[3] Tersoff J, Teichert C and Lagally M G 1996 *Phys. Rev. Lett.* **76** 1675
[4] Xie Q, Madhukar A, Chen P and Kobayashi N P 1995 *Phys. Rev. Lett.* **75** 2542
[5] See also:
McKane A, Droz M, Vannimenus J and Wolf D (ed) 1995 *Scale Invariance, Interfaces, and Non-Equilibrium Dynamics (NATO ASI Series B, vol 344)* (Dordrecht: Kluwer)
[6] de Miguel J J, Cebollada A, Gallego J M, Ferrón J and Ferrer S 1988 *J. Cryst. Growth* **88** 442
[7] Camarero J, de la Figuera J, de Miguel J J, Miranda R, Álvarez J and Ferrer S 2000 *Surf. Sci.* **459** 191
[8] Camarero J, Ferrón J, Cros V, Gómez L, Vázquez de Parga A L, Gallego J M, Prieto J E, de Miguel J J and Miranda R 1998 *Phys. Rev. Lett.* **81** 850
[9] Hoinkes H 1980 *Rev. Mod. Phys.* **52** 933
[10] Engel T and Rieder K H 1982 *Structural Studies of Surfaces with Atomic and Molecular Beam Diffraction* (Berlin: Springer)
[11] Poelsema B and Comsa G 1989 *Scattering of Thermal Energy Atoms (Springer Tracts in Modern Physics vol 115)* (Berlin: Springer)
[12] Esbjerg N and Nørskov J K 1980 *Phys. Rev. Lett.* **45** 807
[13] Hamann D 1981 *Phys. Rev. Lett.* **46** 1227
[14] Harris J and Liebsch A 1982 *Phys. Rev. Lett.* **49** 341
[15] Gómez L J, Bourgeal S, Ibáñez J and Salmerón M 1985 *Phys. Rev.* B **31** 2551
[16] de Miguel J J, Sánchez A, Cebollada A, Gallego J M, Ferrón J and Ferrer S 1987 *Surf. Sci.* **189–l90** 1062
[17] Liebsch A, Harris J, Salanon B and Lapujoulade J 1982 *Surf. Sci.* **123** 338
[18] Poelsema B, de Zwart S T and Comsa G 1982 *Phys. Rev. Lett.* **49** 578
Poelsema B, de Zwart S T and Comsa G 1983 *Phys. Rev. Lett.* **51** 522
[19] Verheij L K, Poelsema B and Comsa G 1985 *Surf. Sci.* **162** 858
[20] Sánchez A and Ferrer S 1987 *Surf. Sci.* **187** L587
[21] Comsa G 1979 *Surf. Sci.* **81** 57
[22] Frank F C and van der Merwe J H 1949 *Proc. R. Soc.* A **198** 205
Frank F C and van der Merwe J H 1949 *Proc. R. Soc.* A **198** 216
Frank F C and van der Merwe J H 1949 *Proc. R. Soc.* A **200** 125
[23] Gronwald K D and Henzler M 1982 *Surf. Sci.* **117** 180
[24] Neave J H, Joyce B A, Dobson P J and Norton N 1983 *Appl. Phys.* A **31** 1
[25] Cohen P I, Petrich G S, Pukite P R and Whaley G J 1989 *Surf. Sci.* **216** 222
[26] Ehrlich G and Hudda F G 1966 *J. Chem. Phys.* **44** 1039
[27] Schwoebel R J and Shipsey E J 1966 *J. Appl. Phys.* **37** 3682
[28] Stoyanov S 1989 *J. Cryst. Growth* **94** 751
[29] Webb M B and Lagally M G 1973 *Solid State Physics* vol 28 (New York: Academic) p 301
[30] Burton W K, Cabrera N and Frank F C 1951 *Phil. Trans. R. Soc.* **243** 299
[31] Ferrón J, de Miguel J J, de la Figuera J, Prieto J E, Camarero J, Cros V and Miranda R 1996/97 *Bulg. Chem. Commun.* **29** 558
[32] Foiles S M, Baskes M I and Daw M S 1986 *Phys. Rev.* B **33** 7993
[33] Yu B D and Scheffler M 1996 *Phys. Rev. Lett.* **77** 1095
[34] Gölzhäuser A and Ehrlich G 1996 *Phys. Rev. Lett.* **77** 1334
[35] Kallinteris G C, Evangelakis G A and Papanicolaou N I 1996 *Surf. Sci.* **369** 185
[36] Bales G S and Zangwill A 1990 *Phys. Rev.* B **41** 5500
[37] Das Sarma S 1998 *Morphological Organization in Epitaxial Growth and Removal (Series on Directions in Condensed Matter Physics vol 14)* (Singapore: World Scientific) p 94 ff
[38] Barabási A-L and Stanley H E 1995 *Fractal Concepts in Surface Growth* (Cambridge: Cambridge University Press)
[39] Das Sarma S and Tamborenea P I 1991 *Phys. Rev. Lett.* **66** 325
[40] Prieto J E, de la Figuera J and Miranda R 2000 *Phys. Rev.* B **62** 2126
[41] Karimi M, Tomkowski T, Vidali G and Biham O 1995 *Phys. Rev.* B **52** 5364
[42] Li Y and DePristo A E 1996 *Surf. Sci.* **351** 189
[43] Liu C L, Cohen J M, Adams J B and Voter A F 1991 *Surf. Sci.* **253** 334
[44] Venables J A 1973 *Phil. Mag.* **27** 693
[45] Gómez L, Slutzky C, Ferrón J, de la Figuera J, Camarero J, Vázquez de Parga A L, de Miguel J J and Miranda R 2000 *Phys. Rev. Lett.* **84** 4397
[46] de la Figuera J, Prieto J E, Ocal C and Miranda R 1993 *Phys. Rev.* B **47** 13 043
[47] de la Figuera J, Huerta-Garnica M A, Prieto J E, Ocal C and Miranda R 1995 *Appl. Phys. Lett.* **60** 1006
[48] de la Figuera J, Prieto J E, Ocal C and Miranda R 1993 *Surf. Sci.* **307–9** 538

[49] Rabe A, Memmel N, Steltenpohl A and Fauster T 1994 *Phys. Rev. Lett.* **73** 2728
[50] Khalil J, Bozzolo G, Farías D, Vázquez de Parga A L, de Miguel J J and Miranda R 2002 *Fall MRS Meeting Proceedings* vol 696, ed E Stach, E Chason, R Hull and S Bader at press
[51] Vázquez de Parga A L, García-Vidal F J and Miranda R 2000 *Phys. Rev. Lett.* **85** 4365
[52] Camarero J, de Miguel J J, Miranda R, Raposo V and Hernando A 2001 *Phys. Rev.* B **64** 125406
[53] Wulfhekel W, Lipkin N N, Kliewer J, Rosenfeld G, Jorritsma L C, Poelsema B and Comsa G 1996 *Surf. Sci.* **348** 227
[54] Speller S, Degroote S, Dekoster J, Langouche G, Ortega J E and Närmann A 1998 *Surf. Sci.* **405** L542
[55] Villarba M and Jónsson H 1994 *Surf. Sci.* **317** 15
[56] Cabrera N and Vermilyea D A 1958 *The Growth of Crystals from Solution* (New York: Wiley) p 393
[57] Henrion J and Rhead G E 1972 *Surf. Sci.* **29** 20
[58] de Beauvois C, Girard Y, Pérard C, Croset B and Mutaftschiev B 1996 *Surf. Sci.* **367** 129
[59] Mansfield M and Needs R J 1991 *Phys. Rev.* B **43** 8829
[60] Mezey L Z and Giber J 1982 *Japan. J. Appl. Phys.* **21** 1569
[61] Ferrón J, Gómez L, Gallego J M, Camarero J, Prieto J E, Cros V, Vázquez de Parga A L, de Miguel J J and Miranda R 2000 *Surf. Sci.* **459** 135
[62] Camarero J, Spendeler L, Schmidt G, Heinz K, de Miguel J J and Miranda R 1994 *Phys. Rev. Lett.* **73** 2448
[63] Kellogg G and Feibelman P J 1990 *Phys. Rev. Lett.* **64** 3143
[64] Feibelman P J 1990 *Phys. Rev. Lett.* **65** 729
[65] Camarero J, de Miguel J J and Miranda R 2002
[66] Prieto J E, Rath Ch, Müller S, Hammer L, Heinz K and Miranda R 2000 *Phys. Rev.* B **62** 5144